Concentration dependence of the up- and down-conversion emission colours of Er(3+)-doped Y2O3: a time-resolved spectroscopy analysis.

Lu, H; Gillin, WP; Hernández, I

Concentration dependence of the up- and down-conversion emission colour of Er^{3+}-doped Y_2O_3; a time-resolved spectroscopy analysis

Haizhou Lu[a], Ignacio Hernández[b]* and William P. Gillin[a,c]*

[a] School of Physics and Astronomy, Queen Mary University of London, Mile End Road, London, E1 4NS, UK

[b] Dpto. CITIMAC, Universidad de Cantabria, Facultad de Ciencias, Avda. Los Castros, s/n 39005, Santander, Spain.[c] College of Physical Science and Technology, Sichuan University, Chengdu, 610064, People's Republic of China

Abstract

In this paper, a series of Er^{3+}-doped Y_2O_3 samples are systematically investigated, focusing on the effect of the doping concentration on the emission lifetime and spectrum under both 488 nm and 980 nm excitations. Decay times of the $^4S_{3/2}$ and $^4F_{9/2}$ emitting states under 488 nm and 980 nm excitations are found to be different and concentration dependent. We explain these variations in terms of the changes in the up-conversion routes caused by the predominance of energy exchanges that involve the lowest lying excited states.

Introduction

Lanthanide doped up-conversion (UC) materials, which can convert infrared radiation into visible luminescence via excited state absorption (ESA) or energy transfer (ET) to excited states, have been widely investigated since their discovery in the 1960s [1-3]. Lanthanide doped UC materials can be used for a variety of applications [2], ranging from biology to solar conversion; the narrow visible emission excited by low energy can be employed in biomedicine [4], solid state laser [5] and illumination [6], and the materials can be implemented in a functional phosphor layer to improve the efficiency of solar cell by means of converting infrared light, which cannot be absorbed by solar cell, into absorbable visible light [7-8].

Although the energy of the excitation and emission bands, due to optical transitions within the $4f^n$ energy manifolds, are weakly dependent on the lanthanide ion's surroundings, changes in the host matrix may affect the emission intensity as well as the UC routes. Lanthanide based UC halides [9-14], glasses [15-16] and oxides [17-24] have been studied both for a basic understanding of the underlying physics and for a number of applications. However, it has been a challenge to find the most chemically stable and efficient material. Beta phase $NaYF_4$ is one of the most studied materials [9-12], as it yields one of the highest UC efficiency [25]. However, it requires a complex synthesis method and it is chemically unstable, which makes it less practical for industrial applications. On the contrary, Y_2O_3 has an excellent chemical stability [23] and the synthesis is simple. Y_2O_3 also has a low phonon energy (430-550 cm^{-1}), which makes it a suitable and practical prototype UC material [24]. Er^{3+}-doped Y_2O_3 UC systems have been previously investigated [17-19]. These studies were presided by a twofold objective: to understand the UC mechanisms upon different excitation wavelengths and the changes in light emission colour upon changes in the erbium concentration or excitation. However, current understanding still involves an ambiguous combination of cross relaxation (CR) processes (two-ion energy transfer involving excited states) and UC routes.

The UC emission colour (that is, the ratio between the different emission bands) as a function of composition is a phenomenon of high interest, as it should allow the material use for multicolour applications. J. A. Capobianco *et al.* reported that the green to red ratio decreases via UC at an excitation wavelength of 815 nm with increasing erbium concentration in Er^{3+}-doped Y_2O_3 system. The change was explained by the occurrence of CR via: $[^4I_{9/2}, {}^4I_{11/2}] \rightarrow [^4I_{13/2}, {}^4F_{9/2}]$ [18]. However, the difference of emission spectra under short excitation wavelength (488 nm) and UC pumping (815 nm) cannot be explained by this mechanism only. The same group postulated that the CR process: $[^4F_{7/2}, {}^4I_{11/2}] \rightarrow [^4F_{9/2}, {}^4F_{9/2}]$ populates the red-emitting state by depopulating the green ones with UC pumping (980 nm) [19] causing a systematic difference of emission spectra under 488 nm and 980 nm excitations. However, this CR process happens under both 488 nm and 980 nm excitations, thus the theory is not enough to explain the spectrum difference. We thus believe that these incomplete models need further testing, clarification and refinement through the insight provided by the population and de-population dynamics. It is also worth noting that despite the great activity and interest in co-doped systems with ytterbium sensitizer and erbium emitters, the green to red ratio changes observed with varying both erbium and ytterbium concentrations have not yet been clearly and unambiguously explained [12]. This is in part due to the lack of dynamic data and the difficulty in modelling so many states and ions. Therefore, we expect our work in the simpler Er^{3+} system to contribute to understanding more practical systems, such as the Yb/Er co-doped material.

In order to fully understand the UC mechanism and emission colour change, and give some fundamental information for co-doped systems, we have performed a study of the Er^{3+}-doped Y_2O_3 system using time resolved spectroscopy, which allows the recording of each emitting state's time decay profile and is a method to understand

the character of the emitting states [20]. The decay times of the emitting states offer the possibility to quantify not only the probability of radiative processes but, importantly, that for non-radiative processes such as CR, which are critical to determine dynamical processes and colour properties of optical materials. Moreover, information can be obtained on the populating mechanisms. To the best of our knowledge, there has been no such a systematic study of the $^4I_{11/2}$ and $^4I_{13/2}$ lifetimes in Y_2O_3 under both 488 nm and 980 nm excitations, which are vital to understand UC processes in this material and in co-doped systems [8, 20].

Experimental

Synthesis of Er^{3+}-doped Y_2O_3 materials

$Y(NO_3)_3{\cdot}6H_2O$ (99.98%) and $Er(NO_3)_3{\cdot}6H_2O$ (99.98%) were purchased from Alfa Aesar. Er^{3+}-doped Y_2O_3 was synthesized through a conventional spray pyrolysis technique. Typically, a mixture of(1-x)M $Y(NO_3)_3{\cdot}6H_2O$ and x M $Er(NO_3)_3{\cdot}6H_2O$ was dissolved in 50 ml de-ionized water. The solution was sprayed, using a conventional spray gun, onto a piece of glass, which was heated to 450 °C on a hotplate creating a uniformly distributed white powder film of Er^{3+}-doped Y_2O_3. The white film was then removed and annealed in a furnace at 1000 °C for 2 hours to produce moisture-free material. A systematic lifetime study under different annealing temperatures and time is given in supplemental information (SI), which shows the optimum annealing conditions.

Instrumentation

Powder X-ray diffraction (XRD) patterns of the dried powders were recorded using Cu Kα radiation (λ=1.5418 Å). The erbium doping concentration was confirmed by energy dispersive X-ray spectroscopy (EDX) at an accelerating voltage of 20 kV.

For the down-conversion (DC) lifetime and spectral measurements, a Continuum Panther optical parametric oscillator (OPO) was used to provide ~7 ns pulse at a wavelength of 488 nm. Also, a 405 nm CW laser was used to investigate the pluse length effect. The fluorescence was dispersed in a Triax 550 spectrometer (gratings: 1200 and 600 lines/mm) and detected by a Hamamatsu R5509-72 photomultiplier.

For the UC lifetime measurement, a 980 nm continuous wave (CW) diode laser was used, which was modulated at a frequency of 11 Hz. The excitation laser was removed from the fluorescence using a short pass filter (10SWF-950-B) which was dispersed and collected using the same system as for the DC measurements.

Results and discussion

Structural characterization

The as synthesised Er^{3+}-doped Y_2O_3 is a pure single cubic phase [26]. XRD data of all Er^{3+}-doped Y_2O_3 materials are shown in figure 1.

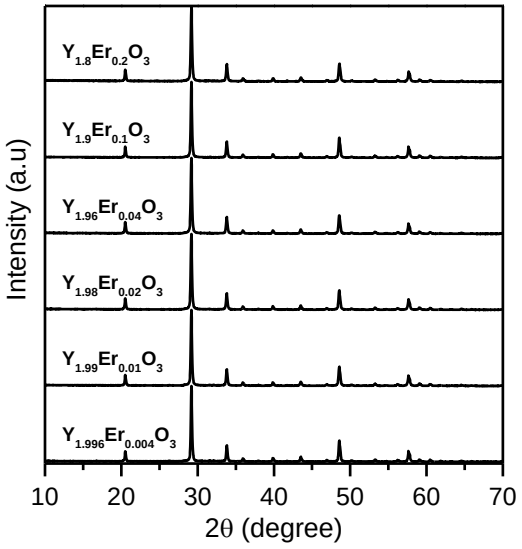

Figure 1. Powder XRD patterns of Er^{3+}-doped Y_2O_3 with various doping concentrations (0.2% to 10%) after annealing at 1000 °C for 2 hours.

EDX spectra were taken for three of the selected samples (0.2%, 5% and 10% Er^{3+}-doped Y_2O_3) and the concentrations of erbium and yttrium were measured to be those of the nominal values. EDX data is shown in the supporting information.

Lifetime measurements

Er^{3+}-doped Y_2O_3 powder yields a wide range of light emission, with discrete bands ranging from the visible (~520 nm) to the infrared (~1535 nm) following the blue excitation at room temperature. In addition, laser illumination at 980 nm is able to excite the visible bands through UC processes. The bands, shown in figure 2 for 0.2% Er^{3+}-doped Y_2O_3, can be assigned to the corresponding emissions from the $^4S_{3/2}$, $^4F_{9/2}$, $^4I_{11/2}$ and $^4I_{13/2}$ states to the ground $^4I_{15/2}$ state.

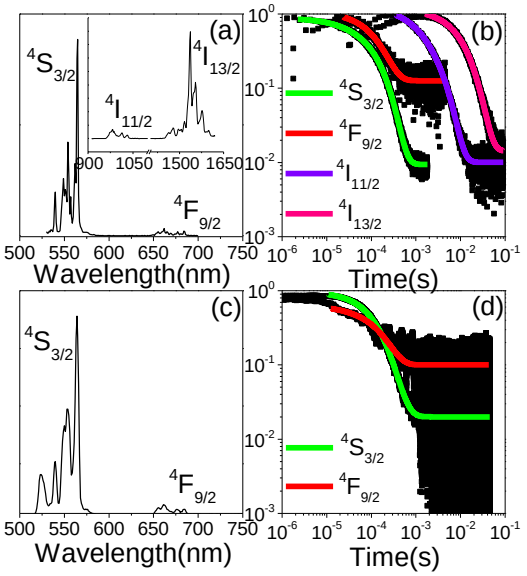

Figure 2. (a) Spectra of 0.2% Er^{3+}-doped Y_2O_3 under 488 nm excitation, (b) I_t curves of all emitting states of 0.2% Er^{3+}-doped Y_2O_3 under 488 nm excitation, (c) Spectra of 0.2% Er^{3+}-doped Y_2O_3 under 980 nm excitation, (d) I_t curves of all visible emitting states of 0.2% Er^{3+}-doped Y_2O_3 under 980 nm excitation.

As we have stated in the introduction, spectral information is not, by itself, sufficient to understand the difference between DC and UC processes as it only provides a partial picture. In order to fully understand the occurring processes, it is necessary to obtain the details of the decay curves of all intervening states showing how each state is populated and depopulated. All the decay curves, I_t were fitted with a double exponential equation,

$$I_t = \mathrm{A}_1 * \exp\left(\frac{-\mathrm{t}}{\tau_1}\right) + \mathrm{A}_2 * \exp\left(\frac{-\mathrm{t}}{\tau_2}\right) \quad (1)$$

where I_t is the decaying intensity at the maximum of the emission band, A_1, A_2 are the exponential pre-factors and τ_1 and τ_2 are the fitted decay times. This model is usually employed to account for the decay of erbium ions in an inhomogeneous environment, for example where ions are either in the bulk or near the surface and undergoing different quenching or energy transfer routes or when a population of the ions is close to the presence of impurities. The average decay time constant $\mathrm{t_{av}}$ can be determined using [13],

$$\mathrm{t_{av}} = \frac{\mathrm{A}_1{\tau_1}^2 + \mathrm{A}_2{\tau_2}^2}{\mathrm{A}_1\tau_1 + \mathrm{A}_2\tau_2} \quad (2)$$

Figure 2(b) shows the recorded decay curves of the $^4S_{3/2}$, $^4F_{9/2}$, $^4I_{11/2}$ and $^4I_{13/2}$ states for the 0.2% Er^{3+}-doped Y_2O_3 sample. The $^4S_{3/2}$ and $^4F_{9/2}$ emitting states (green and red emissions, respectively) show relatively short average DC lifetimes, t_{av} < 120 µs, while the IR emitting states, $^4I_{11/2}$ and $^4I_{13/2}$, present lifetimes more than ten times longer, in the order of milliseconds. These long-lived $^4I_{11/2}$ and $^4I_{13/2}$ states can, in principle, act as intermediate states for further excitation under 980 nm excitation or participate in energy transfer processes between close erbium ions, causing the visible UC (figure 2c).

In the given excitation conditions, 0.2% Er^{3+}-doped Y_2O_3 shows the longest DC lifetimes along the $Y_{2-x}Er_xO_3$ series for all the emitting states ; this is caused by the reduced non-radiative mechanisms for this dilution and particularly the small contribution of concentration-derived quenching such as CR. The fact that the average UC decay time (~ 150 µs) is similar to the DC average lifetime (~ 120 µs) proves that energy transfer UC (ETU) is extremely restricted. In the general case, if the UC is only due to ESA, the $^4F_{7/2}$ emitting level is populated through the energy resonant $^4I_{11/2} + h\upsilon \rightarrow {}^4F_{7/2}$ process and the subsequent rapid relaxation to the green emitting levels ($^2H_{11/2}$ and $^4S_{3/2}$); therefore, the emission processes are exactly the same as under 488 nm excitation. Figure 3, shows a much more significant difference between UC and DC average decay times for Er^{3+} concentrations higher than 0.5 %. For these concentrations, the average lifetimes of $^4S_{3/2}$ and $^4F_{9/2}$ emitting states under 980 nm excitation are in the order of hundreds of microseconds, while the DC lifetimes are considerably shorter. These much higher values and differences constitute a direct evidence that the dominant UC mechanism under 980 nm excitation for high erbium concentrations is ETU involving the long lived $^4I_{11/2}$ and $^4I_{13/2}$ states as excitation reservoirs. ETU processes imply a modulation of the emission lifetime by the long-lived states acting as a reservoir [18,20]. The occurrence of ETU means that erbium-erbium interactions are present even at 0.5 % Er^{3+} content and therefore, if we discard aggregation, the erbium-erbium interaction distance can be estimated to be higher than 150 nm.

In the case of 0.2% Er-doped Y_2O_3, itis noteworthy that the green to red emission ratio is also very similar in the case of UC and DC spectra (figures 2a and 2b). This difference between UC and DC spectra is much more significant for the higher concentrations).

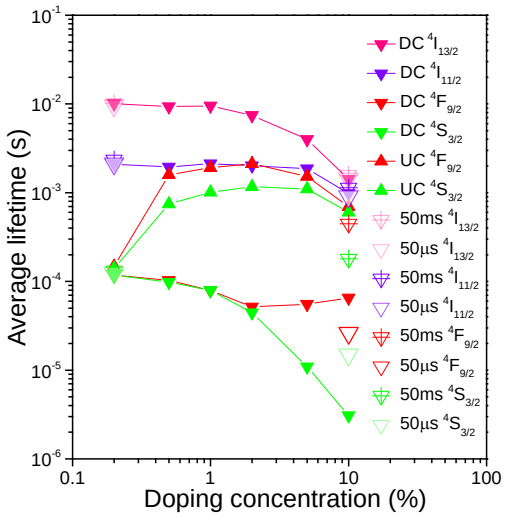

Figure 3. Average decay lifetime of all emitting states of all Er^{3+}-doped Y_2O_3 during DC and UC processes (see text for excitation conditions). Note that DC times overlap irrespective of excitation wavelength or pulse length.

Figure 3 summarizes the average lifetimes for the Er^{3+}-doped Y_2O_3 series when varying the doping concentration from 0.2, to 10 % for both the UC (excitation at 980 nm) and DC (pulsed excitation at 488 nm). Importantly, before discussing the average lifetime dependence of the emissions with the Er^{3+} concentration we must note here that the DC and UC time-resolved I_t curves were measured with different excitation lasers: a pulsed 488 nm laser allowing for the measurement of the intrinsic population and depopulation for DC and a 980 nm CW laser, needed to achieve detectable UC, respectively. In order to study the effect of the excitation pulse length in the difference between DC and UC dynamics we also measured the I_t decay curves for the DC with different excitation pulse lengths by employing a modulated 405 nm CW laser and varying the laser power for the 488 nm laser pulse for the most diluted and most concentrated samples. The average decay times measured for 50 µs and

50 ms, 405 nm excitation pulses on 0.2% and 10 % Er^{3+}-doped Y_2O_3 are also included in Figure 3. We observe in the figure that for all DC emission wavelengths the average lifetimes for the 0.2% Er^{3+} are irrespective of the laser pulse length. This is also an evidence for the absence of energy transfer, as we will comment later. The lifetimes of the longer-lived IR emissions also show no dependence with the excitation length in the case of the 10 % Er^{3+}-doped Y_2O_3. The green emission, however, shows an increased average lifetime for the 405 nm, 50 µs excitation pulses, which is almost an order of magnitude higher with respect to the 488 nm, 7 ns excitation, and reaches up to two orders of magnitude higher value for the 405 nm, 50 ms excitation. The red emission shows a decrease in the lifetime for the 50 µs long excitation, approximating the green emission lifetime, but experiences an increase for the 50 ms excitation, taking almost the same value as for UC (see SI for numerical values). Interestingly, 405 nm, 500 µs pulse duration excitation provides an intermediate value of 76 µs for the $^4F_{9/2}$ DC emission, close to the 65 µs obtained for 488 nm pulsed excitation. A similar dependence with the laser power has been observed upon varying the energy of the OPO laser pulses (see SI). Figure 3 shows that the average DC lifetimes of the $^4I_{13/2} \rightarrow {}^4I_{15/2}$ and $^4I_{11/2} \rightarrow {}^4I_{15/2}$ transitions experience a monotonous lifetime decrease when increasing the erbium concentration. This can be explained in terms of concentration dependent non-radiative theory [13]. Concentration dependent non-radiative decays occur due to the enhancement of energy transfer processes, which include excitation hopping (and may lead the excitation to non-radiative traps) and CR mechanisms involving the emitting levels, both becoming more likely as the average distance between Er^{3+} ions is reduced. Some of the CR mechanisms (which may be resonant or vibrationally assisted) include the cooperative non-radiative decays $[^4I_{11/2}, {}^4I_{11/2}] \rightarrow [^4F_{7/2}, {}^4I_{15/2}]$, $[^4I_{11/2}, {}^4I_{13/2}] \rightarrow [^4F_{9/2}, {}^4I_{15/2}]$, $[^4F_{7/2}, {}^4I_{11/2}] \rightarrow [^4F_{9/2}, {}^4F_{9/2}]$ and $[^4I_{13/2}, {}^4I_{13/2}] \rightarrow [^4I_{11/2}, {}^4I_{15/2}]$ as represented in figure 4. In fact, some of these processes contribute to the ETU.

Figure 3 also shows that under 980 nm excitation (UC regime), the lifetimes of the $^4S_{3/2}$ and $^4F_{9/2}$ emitting states show a similar trend. They both increase as the doping concentration increases from 0.2% to 2%. At higher doping concentrations there is a subsequent decrease in the lifetime. This variation emphasizes that the dynamics of the reservoir and transfer govern the decay of the UC emission [18, 20]. Interestingly, figure 3 shows that the UC lifetime of the $^4F_{9/2}$ (red) emitting state in the intermediate concentration regime 0.5-5 % is considerably longer (approximately twice as long) than that of $^4S_{3/2}$ emitting state. However, the DC lifetime measured under 488 nm excitation is almost the same in the case of erbium dilutions below 2%. Thus, it can be concluded that there are different energy transfer processes populating the $^4S_{3/2}$ and $^4F_{9/2}$ emitting states, respectively. The longer average lifetime for the red emission suggests that the states feeding $^4F_{9/2}$ are correspondingly longer-lived than those for the green emission, implying that the energy transfer, $[^4I_{11/2}, {}^4I_{13/2}] \rightarrow [^4F_{9/2}, {}^4I_{15/2}]$ is relevant in ETU in the more concentrated systems of the studied series. Moreover, the incidence of this CR route in the re-population of the $^4F_{9/2}$ even in the DC regime (together with the $[^4I_{13/2}, {}^4I_{13/2}] \rightarrow [^4I_{9/2}, {}^4I_{15/2}]$ CR [27, 28], which repopulates the $^4I_{9/2}$ reservoir), explains the increase of the red DC emission lifetime observed in the high concentration Er^{3+}-doped Y_2O_2 when the population of the $^4I_{11/2}$ and $^4I_{13/2}$ states is large (figure 3). This model has implications in the changes of the red to green emission colour ratios as a function of power, concentration and excitation wavelength (DC or UC).

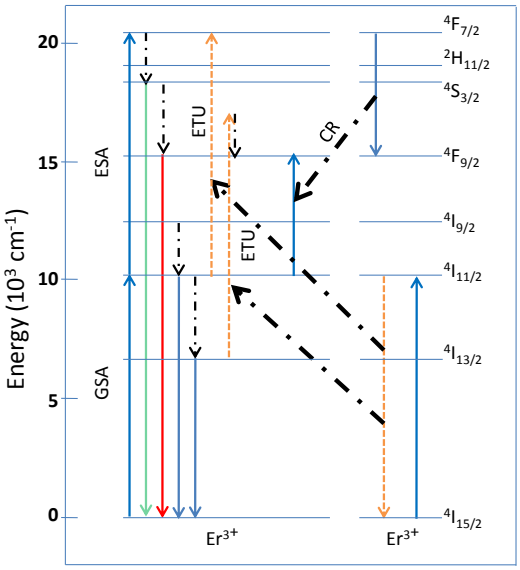

Figure 4. Simplified energy level diagram and most relevant radiative and energy transfer mechanisms in Er^{3+}-doped Y_2O_3. Ground state absorption (GSA), excited state absorption (ESA), green, red and IR luminescence, and energy transfer UC (ETU) as well as cross relaxation (CR) are presented.

The lifetime study can be summarized as follows: (1), the IR emitting states $^4I_{11/2}$ and $^4I_{13/2}$ experience a systematic lifetime decrease with increasing doping concentration, which we assign to conventional concentration quenching (i.e. hopping and CR). This quenching gets more severe as the concentration increases and has important implications in the visible photoluminescence, as this levels act as excitation reservoirs due to their long lifetime, in the order of millisconds. (2), under 980 nm excitation, the lifetime increases from 0.5% to 2% and then decreases from 2% to 10%. The first increase is due to the UC route change from a situation in which ESA is the main mechanism to a prevalence of ETU involving the well-known $[^4I_{11/2}, {}^4I_{11/2}] \rightarrow [^4F_{7/2}, {}^4I_{15/2}]$. The subsequent decrease with increasing erbium concentration is predominantly caused by the shortened IR intrinsic lifetime. (3), other CR routes, including mainly $[^4I_{11/2}, {}^4I_{13/2}] \rightarrow [^4F_{9/2}, {}^4I_{15/2}]$ and looping mechanisms that re-populate the upper excited states for high concentrations and high powers for both the UC and DC regimes.

Difference between up-conversion and down-conversion spectra

The emission spectra under 488 nm and 980 nm excitations are shown in figure 5(a). The green to red ratio decreases with increasing erbium concentration under both 488 nm and 980 nm excitations, but follows a different trend as showed in figure 5(b). Under 488 nm OPO excitation (DC), the green to red ratio change is small from 0.2% to 1% erbium doping concentration, while it decreases a factor 10 from 1% to 10% erbium doping concentration. However, for the 980 nm excitation, it decreases considerably more over the 0.2% to 1% concentration range with comparatively little subsequent change.

Concentration-induced processes, which affect the population (and decay) of $^4S_{3/2}$ and $^4F_{9/2}$ states differently, explain the change in the DC and UC spectra in the explored power regime. Upon direct excitation on the $^4F_{7/2}$ state, the CR-induced changes in the population are not significant from 0.2 % to 1% and, as observed in figure 3, neither are the decay processes. From 1 % to 10 %, as concentration quenching becomes significant and a severe CR including the processes $[^4I_{11/2}, {}^4I_{13/2}] \rightarrow [^4F_{9/2}, {}^4I_{15/2}]$ and $[^4F_{7/2}, {}^4I_{11/2}] \rightarrow [^4F_{9/2}, {}^4F_{9/2}]$ and the looping mechanisms for high populations of the IR states start to occur, the red emission becomes comparatively more intense than the green one.

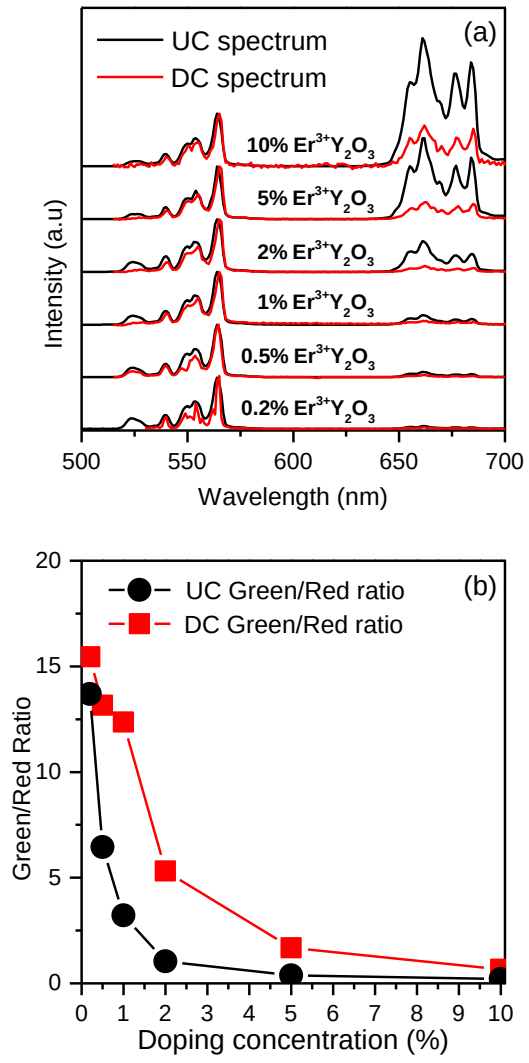

Figure 5. (a) Spectra under both 980 nm (UC) and 488 nm (DC) excitations; (b) Green to red ratio change with doping concentration for UC and DC processes.

The change in the UC routes explains the change in the emission spectrum for the 980 nm excitation UC regime. At 0.2% doping concentration, ESA is the significant UC route, the spectrum being very similar to that observed under 488 nm excitation. With increasing erbium concentration, ETU gets more preponderant. The ETU process $[^4I_{11/2}, {}^4I_{11/2}] \rightarrow [^4F_{7/2}, {}^4I_{15/2}]$ contributes to populate the upper states as the ESA or similarly to the DC regime, but the other CR and looping mechanisms described above and, especially the cooperative non-radiative decay $[^4I_{11/2}, {}^4I_{13/2}] \rightarrow [^4F_{9/2}, {}^4I_{15/2}]$ result in a higher nominal population of $^4F_{9/2}$. Thus, there is a steady increase of red emission with increasing concentration from 0.2% to 10%.

Conclusions

We have studied the UC mechanisms in the simple Er^{3+}-doped Y_2O_3 system as a function of the Er^{3+} concentration through the change in the dynamics of the emitting states, including the $^4I_{11/2}$ and $^4I_{13/2}$ states. We have done this by employing different excitation powers, pulse lengths and wavelengths. We have described the progressive importance of energy transfer and CR as the Er^{3+} content increases from 0.2% to 10% and its implications in the spectral properties and decay times of the UC (excitation at 980 nm) but also for DC. These processes, including looping mechanisms result in an increase of the DC decay time for high Er^{3+} concentration in given excitation powers. Moreover they cause a dominance of the population of the red emitting state for UC at high Er^{3+} concentrations, thus affecting severely the green to red emission ratio.

The understanding of the doping concentration dependent population and decay routes would allow implementing this material with tailored emitting colour properties for phosphors, display and biological applications. Using this approach it would also be possible to acquire a deeper insight into more complex, but more practical erbium-ytterbium co-doped systems.

Acknowledgement:

The authors thank Dr. R. Wilson for XRD measurements and Dr. Z. Luklinska for EDX measurements. HL is funded by the China Scholarship Council and Queen Mary University of London. IH acknowledges funding from the EU FP7 (Marie Curie-CIG-Grant 303535).

Reference:

1 V. V. Ovsyankin and P. P. Feofilov, *JETP Lett.*, 1966, **4**, 317.

2 F. Auzel, *Chem. Rev.*, 2004, **104**, 139.

3 F. Vetrone, J. C. Boyer, J. A. Capobianco, *In the Encyclopedia of Nanoscience and Nanotechnology*, 2004, **10**, 725.

4 X. Liu, H. Qian, Y. Ji, Z. Li, Y. Shao, Y. Hu, G. X. Tong, L. Li, W. Guo and H. Guo, *RSC Adv.*, 2012, **2**, 12263.

5 E. Downing, L. Hesselink, J. Ralston, R. Macfarlane, *Science*, 1996, **273**, 1185.

6 J. Zhao, D. Jin, E. P. Schartner, Y. Lu, Y. Liu, A. V. Zvyagin, L. Zhang, J. M. Dawes, P. Xi, J. A. Piper, E. M. Goldys and T. M. Monro, *Nature Nanotechnology*, 2013, **8**, 729.

7 M. Kong, W. Hu, F. Cheng, Z. Huang, J. Zhang, Z. Han, N. Shi, Q. Fan, S. Chen and W. Huang, *J. Mater. Chem. C.*, 2013, **1**, 5872.

8 R. M. Rodríguez, S. Fischer, A. Ivaturi, B. Froehlich, K. W. Krämer, J. C. Goldschmidt, B. S. Richards, and A. Meijerink, *Chem. Mater.*, 2013, **25**, 1912.

9 F. Wang, Y. Han, C. S. Lim, Y. Lu, J. Wang, J. Xu, H. Chen, C. Zhang, M. Hong and X. Liu, *Nature*, 2010, **463**, 1061.

10 J. Wang, H. Song, W. Xu, B. Dong, S. Xu, B. Chen, W. Yu and S. Zhang, *Nanoscale*, 2013, **5**, 3412.

11 J. Zhao, Z. Lu, Y. Yin, C. McRae, J. A. Piper, J. M. Dawes, D. Jin and E. M. Goldys, *Nanoscale*, 2013, **5**, 944.

12 H. X. Mai, Y. W. Zhang, L. D. Sun and C. H. Yan, *J. Phys. Chem. C.*, 2007, **111**, 13721.

13 M. C. Tan, G. A. Kumar, R. E. Riman, M. G. Brik, E. Brown and U. Hommerich, *J. Appl. Phys.*, 2009, **106**, 063118.

14 J. W. Stouwdam and F. C. J. M. Veggel, *Nano Lett.*, 2002, **2**, 733.

15 P. S. Golding, S. D. Jackson, T. A. King and M. Pollnau, *Phys. Rev. B.*, 2000, **62**, 856.

16 J. Qiu, P. G. Kazanski, J. Si, K. Miura, T. Mitsuyu, *Appl. Phys. Lett.*, 2000, **77**, 1940.

17 J. A. Capobianco, F. Vetrone, T. D´Alesio, G. Tessari, A. Speghini and M. Bettinelli, *Phys. Chem. Chem. Phys.*, 2000, **2**, 3203.

18 J. A. Capobianco, F. Vetrone and J. C. Boyer, *J. Phys. Chem. B.*, 2002, **106**, 1181.

19 F. Vetrone, J. C. Boyer, J. A. Capobianco, A. Speghini and M. Bettinelli, *Chem. Mater.*, 2003, **15**, 2737.

20 I. Etchart, A. Huignard, M. Bérard, M. N. Nordin, I. Hernández, R. J. Curry, W. P. Gillin and A. K. Cheetham, *J. Mater. Chem.*, 2010, **20**, 3989.

21 Y. Mao, T. Tran, X. Guo, J. Y. Huang, C. K. Shih, K. L. Wang and J. P. Chang, *Adv. Funct. Mater.*, 2009, **19**, 748.

22 E. D. L. R. Cruz, L. A. D. Torres, R. A. R. Rojas, M. A. M. Nava and O. B. García, *Appl. Phys. Lett.*, 2003, **83**, 4903.

23 H. Eilers, *Materials Letters*, 2006, **60**, 214.

24 H. Guo, W. Zhang, L. Lou, A. Brioude and J. Mugnier, *Thin Solid Films*, 2004, **458**, 274.

25 J. F. Suyver, A. Aebischer, S. G. Revilla, P. Gerner and H. U. Güdel, *Phys. Rev. B.*, 2005, **71**, 125123.

26 F. Hanic, M. Hartmanová, G.G. Knab, A.A. Urusovskaya and K.S. Bagdasarov, *Acta Cryst.*, 1984, **B40**, 76.

27 I. Hernández, R. H. C. Tan, J. M. Pearson, P. B. Wyatt, W. P. Gillin, *J. Phys. Chem. B*, 2009, **113**, 7474.

28 L. Agazzi, K. Wörhoff, M. Pollnau, *J. Phys. Chem. C*, 2013, **117**, 6759.